

12-27-1994

## Surface Stress, Morphological Development, and Dislocation Nucleation During SixGe<sub>1-x</sub> Epitaxy

D. E. Jesson

*Oak Ridge National Laboratory, [ejp@solid.ssd.ornl.gov](mailto:ejp@solid.ssd.ornl.gov)*

S. J. Pennycook

*Oak Ridge National Laboratory*

J. -M. Baribeau

*National Research Council of Canada*

D. C. Houghton

*National Research Council of Canada*

Follow this and additional works at: <https://digitalcommons.usu.edu/microscopy>



Part of the [Biology Commons](#)

---

### Recommended Citation

Jesson, D. E.; Pennycook, S. J.; Baribeau, J. -M.; and Houghton, D. C. (1994) "Surface Stress, Morphological Development, and Dislocation Nucleation During SixGe<sub>1-x</sub> Epitaxy," *Scanning Microscopy*. Vol. 8 : No. 4 , Article 11.

Available at: <https://digitalcommons.usu.edu/microscopy/vol8/iss4/11>

This Article is brought to you for free and open access by the Western Dairy Center at DigitalCommons@USU. It has been accepted for inclusion in Scanning Microscopy by an authorized administrator of DigitalCommons@USU. For more information, please contact [digitalcommons@usu.edu](mailto:digitalcommons@usu.edu).



## SURFACE STRESS, MORPHOLOGICAL DEVELOPMENT, AND DISLOCATION NUCLEATION DURING $\text{Si}_x\text{Ge}_{1-x}$ EPITAXY

D.E. Jesson, S.J. Pennycook, J.-M. Baribeau<sup>1</sup> and D.C. Houghton<sup>1</sup>

Solid State Division, Oak Ridge National Laboratory, Oak Ridge, Tennessee 37831-6030

<sup>1</sup>Institute for Microstructural Sciences, National Research Council of Canada, Ottawa, K1A 0R6 Canada

(Received for publication July 15, 1994 and in revised form December 27, 1994)

### Abstract

Utilizing Ge marker layer experiments combined with atomic number contrast (Z-contrast) imaging, we have studied the evolving surface morphology of  $\text{Si}_x\text{Ge}_{1-x}$  alloys during growth by molecular beam epitaxy. The marker layers map out the instability transition between planar two-dimensional (2D) growth and three-dimensional (3D) growth. The transition occurs via the gradual formation of a surface ripple as anticipated from instability theory. However, these undulations rapidly develop into crack-like surface instabilities which we simulate and explain by the mechanism of stress-driven surface diffusion. Finally, we model the large stresses associated with these features within a fracture mechanics formalism. This analysis demonstrates that crack-like instabilities provide ideal candidate sites for the nucleation of misfit dislocations.

**Key Words:** Atomic number contrast (Z-contrast) imaging, morphological instability, dislocation nucleation.

### \*Address for correspondence:

D.E. Jesson  
Oak Ridge National Laboratory,  
P.O. Box 2008,  
Oak Ridge, TN 37831-6030

Telephone number: (615) 574-6281

FAX number: (615) 574-4143

E.mail: [ejp@solid.ssd.ornl.gov](mailto:ejp@solid.ssd.ornl.gov)

### Introduction

The instability of strained epitaxial thin films to the formation of surface waves or undulations has been appreciated for several years (Asaro and Tiller, 1972; Grinfeld, 1986; Srolovitz, 1989; Spencer *et al.*, 1991). Under uniaxial compression, atom planes situated close to the peaks of the undulations can relax relative to the bulk, significantly lowering the stored elastic energy of the film (Fig. 1). This more than compensates for the associated increase in surface energy, provided that the undulation wavelength is greater than

$$\lambda_{\min} = [(2\mu\pi\gamma) / \{(1-\nu)\sigma^2\}]. \quad (1)$$

Here,  $\gamma$ ,  $\mu$ , and  $\nu$  are respectively the surface energy, shear modulus, and Poisson's ratio of the strained film. The wavelength most likely to be observed (i.e., the most dangerous wavelength) is  $\lambda_{\text{obs}} = (4/3)\lambda_{\min}$ .

The peak relaxation in Figure 1 is inevitably accompanied by a compression of the lattice planes at the undulation valleys. These stress concentrations can be large, even for rather small surface perturbations. Gao (1991), for example, has obtained the linearized perturbation solution for the surface stress distribution associated with sinusoidal surface of Figure 1. He found,

$$\sigma_r(x) = \sigma [1 + \{(4\pi A)/\lambda\} \cos\{(2\pi x)/\lambda\}], \quad (2)$$

which reveals that the valley stress doubles for a sinusoidal surface wave amplitude  $A$  equal to only one tenth of its wavelength  $\lambda$ . In this paper, we consider the role of such large surface stresses in the subsequent morphological development of thin films and the potential implications for strain relaxation via the nucleation of misfit dislocations.

### Marker Layer Experiments

In order to study morphological development in the presence of high surface stresses, we have performed a  $\text{Si}_{0.5}\text{Ge}_{0.5}/\text{Si}(100)$  growth experiment in which two

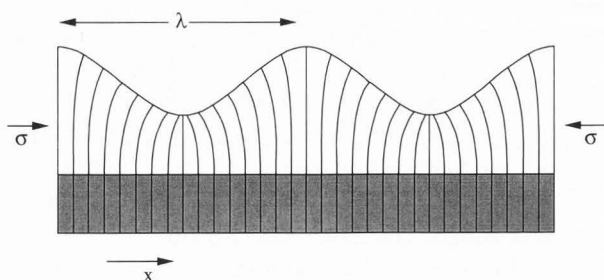


**Figure 1.** Schematic representation of a surface undulation in a thin film subjected to uniaxial compression.

monolayer-thick Ge marker layers were deposited at selected intervals (Jesson *et al.*, 1993a). The marker layers act to map out the far-from-equilibrium surface shapes at a particular instant during growth. Since bulk diffusion is negligible, several marker layers provide a "fossil" or "strata" record of surface evolution (Fig. 2). By fabricating a specimen suitable for cross-sectional imaging of the marker layers, it is then possible to deduce the time evolution of the surface profile.

The atomic number contrast (Z-contrast) imaging technique (Pennycook and Jesson, 1990, 1991) is particularly well suited to imaging Ge marker layers in  $\text{Si}_x\text{Ge}_{1-x}$  alloys. A small 2 Å probe is scanned across the surface of the thin marker layer sample and transmitted electrons scattered through large angles are simultaneously collected by an annular detector which is equipped with a large inner angle (Fig. 3a). The image of the Ge marker in Si (Fig. 3b) is, therefore, built up sequentially as a function of probe position, each bright spot in the image corresponding to a dimer or "dumb-bell" of the [110] projection. The Ge dimers appear brighter than the Si dimers in the image simply because the large-angle scattering cross-sections start to approach the atomic number squared ( $Z^2$ ) dependence of unscreened Rutherford scattering. The technique is, therefore, ideal for imaging marker layers at a variety of magnifications, allowing the study of morphological instability over a wide range of length scales.

It is interesting to note that the marker layer technique would seem to offer significant advantages for the study of far-from-equilibrium growth shapes in the presence of large surface stresses. In particular, it is possible to maintain a high supersaturation throughout the growth experiment, which is important for high misfit films where large stress concentrations can considerably enhance surface diffusion. Thus, marker layer experiments should faithfully map the far-from-equilibrium growth morphology and avoid uncertainties inherent in conventional "quench and look" approaches.

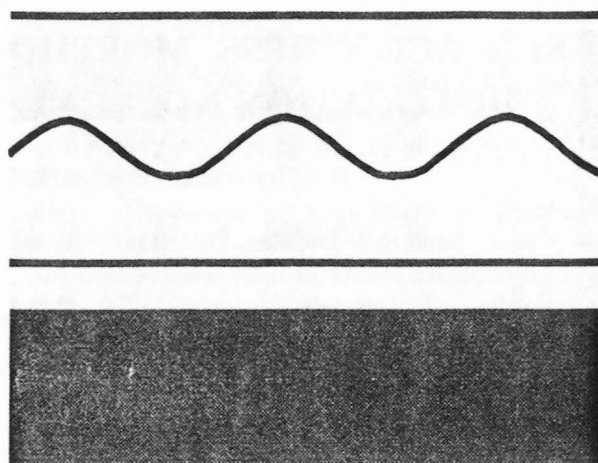


**Figure 2.** A schematic representation of thin Ge marker layers embedded in a  $\text{Si}_{0.5}\text{Ge}_{0.5}$  alloy. Each marker layer maps the far-from-equilibrium surface profile at a particular time during growth.

#### The Kinetic Critical Thickness

A typical experimental result for  $\text{Si}_{0.5}\text{Ge}_{0.5}$  grown at 400°C and  $2 \text{ \AA s}^{-1}$  is contained in Figure 4. The marker layers appear as bright horizontal lines. Initially, the surface morphology is flat until the film is about 25 nm thick, where a ripple morphology can be clearly distinguished. This can be understood as a kinetic critical thickness  $h_k$  at which the strain-driven morphological development has become significant in comparison with the growth rate. Surface rippling is, therefore, kinetically inhibited, which is consistent with the far-from-equilibrium growth conditions.

A quantitative theory of  $h_k$  has recently been given by Spencer *et al.* (1991, 1993) which predicts  $h_k \propto \epsilon^{-8} \lambda^{-2}$  where  $\epsilon$  is the misfit strain and  $\lambda$  the perturbation wavelength. This has been subsequently extended by Guyer and Voorhees (personal communication) to include the effects of elastic stresses created by compositional inhomogeneities in the alloy film. The predictions of  $h_k$  and  $\lambda$  based on this theory for our growth conditions and alloy composition would appear to be in excellent agreement with experiment. Although the calculations are necessarily sensitive to the value of surface diffusion coefficient [the value measured by Chason *et al.* (1990) was used in this case], the agreement would appear to be very promising considering the other severe functional dependencies of the theory. It might, therefore, be hoped that a comparison between experiment and theory in this way will improve our understanding of the essential physics governing morphological instability.

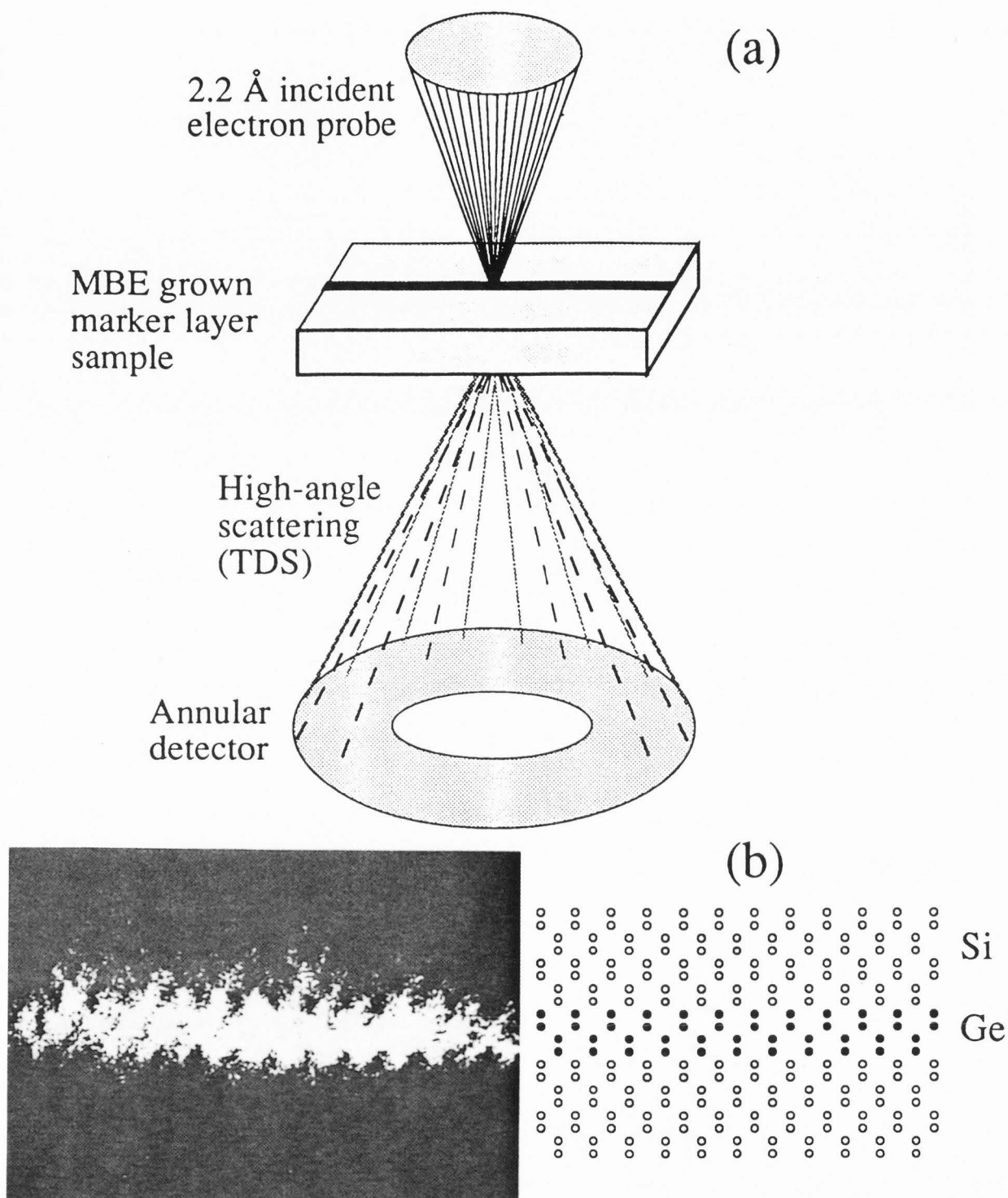
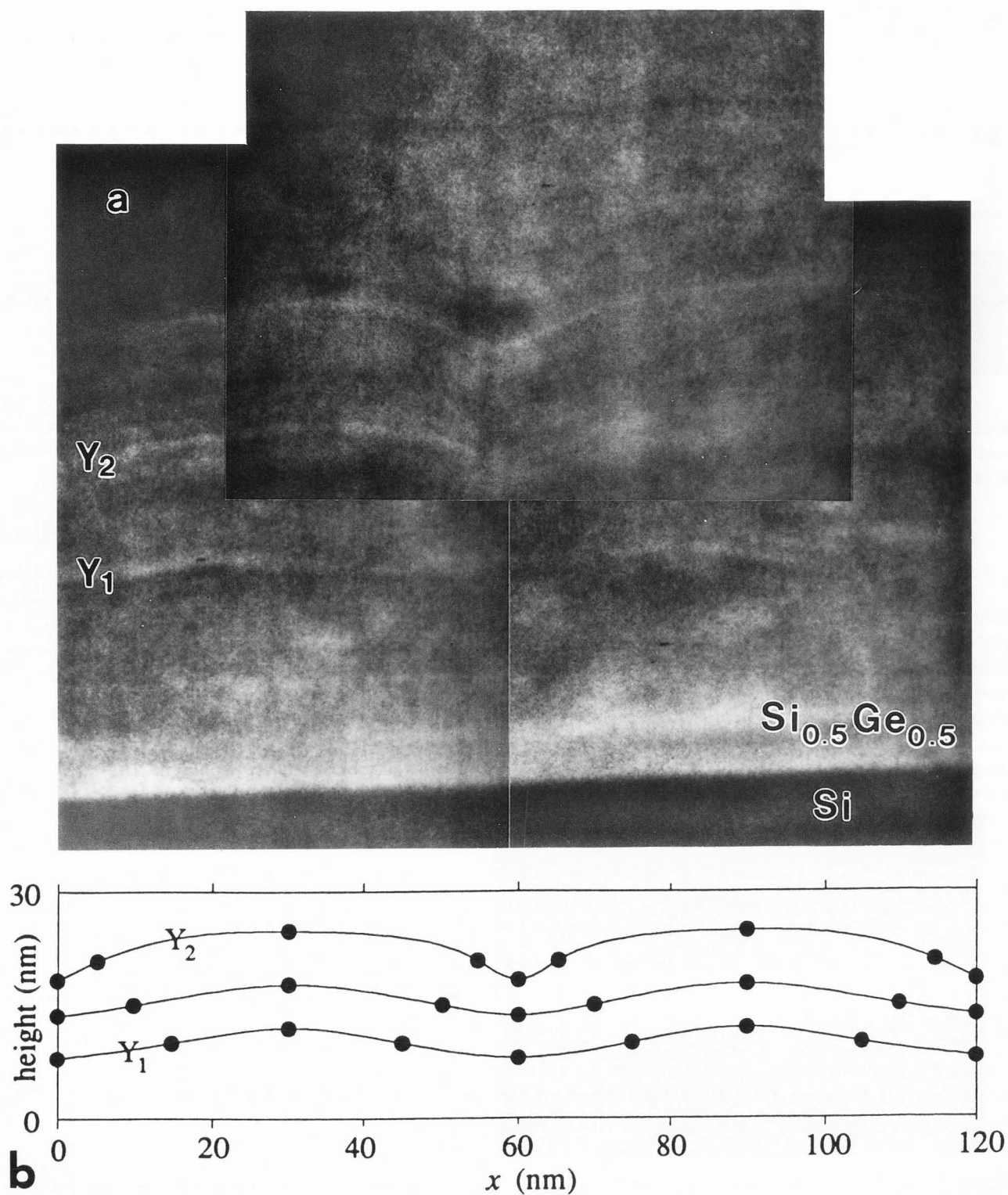


Figure 3. (a) The Z-contrast imaging process. (b) [110] Z-contrast image of a Ge marker layer in Si (see text).

### Nonlinear Surface Instabilities

A surprising consequence of surface evolution beyond the realm of linear perturbation theory is revealed in Figure 4. The surface undulations can rapidly de-

velop into sharp cusps. These features would appear to be highly metastable, persisting for 20 nm or so before rapidly smoothing out. The film then continued to grow with a flat surface morphology (within the sensitivity of the experiment) for the remainder of the deposition.



**Figure 4.** (a) [110] Z-contrast image of a  $\text{Si}_{0.5}\text{Ge}_{0.5}$  alloy grown by molecular beam epitaxy (MBE) at  $400^\circ\text{C}$  and  $2 \text{ \AA s}^{-1}$ . The bright horizontal lines represent 2-monolayer-thick Ge marker layers. The surface profile simulations in (b) correspond to the period of cusp formation in (a) between vertical ordinates  $Y_1$  and  $Y_2$  (see Jesson *et al.*, 1993a).

Given that surface diffusion is driven by gradients in surface chemical potential, the development of a cusp at the valley of a surface wave as represented in Figure 1 is rather intuitive (Jesson *et al.*, 1993a, 1993b). Consider, for example, a diffusing adatom bonding at the valley of a sinusoidal perturbation in the surface. At this location, the atom experiences the greatest stress concentration and would prefer to migrate to the more relaxed regions associated with the peaks. However, diffusion from the valley to the peaks increases both the depth  $d$  and sharpness of the valley ( $1/\rho$ ). This increases the stress concentration  $\approx 1 + 2\sqrt{d/\rho}$  at the valley, which in turn accentuates the rate of migration. It is, therefore, not difficult to anticipate that the limiting morphology will be a cusp, similar to our experimental observations.

These ideas can be shown to be reasonable using a simple model for cusp development (Jesson *et al.*, 1993a). For example, the surface profile simulations in Figure 4b qualitatively reproduce all of the experimental features of cusp formation between  $Y_1$  and  $Y_2$ . Recently, more sophisticated models of surface evolution have also predicted the formation of cusps (Nozières, 1993; Yang and Srolovitz, 1993; Spencer and Meiron, 1994; Chiu and Gao, 1994). It is conceivable that these models combined with marker layer experiments could form the basis for the quantitative study of nonlinear surface instabilities.

An interesting prediction of all the surface evolution models (including the simulation in Fig. 4) is that upon attaining a critical cusp geometry, the stress concentration at the cusp tip increases rapidly. At this point, the cusp accelerates rapidly into the film via the process of stress-enhanced surface diffusion, leading to an interesting comparison between the critical geometry for cusp propagation and the well-known Griffith criterion for the unstable propagation of a crack in a brittle material (Tetelman and McEvily, 1967; Jesson *et al.*, 1993b, 1994; Yang and Srolovitz, 1993). This is probably best appreciated when the cusp is under tensile stress, where it has been suggested that the stress-driven morphological instability may in fact precede and initiate the formation of a critical Griffith crack (Yang and Srolovitz, 1993). In compression, a large stress concentration (a negative mode I stress intensity factor) must also develop because the material on each side of the cusp is not in contact (Chiu and Gao, 1993; Jesson *et al.*, 1993a). This is not true for a slit crack, which will simply close under compression.

The Griffith criterion for the critical crack length required for fracture is (Tetelman and McEvily, 1967)

$$d^* = \{(2E\gamma) / (\pi\sigma^2)\}. \quad (3)$$

For our conditions,  $d^* = 8$  nm, which is very close to

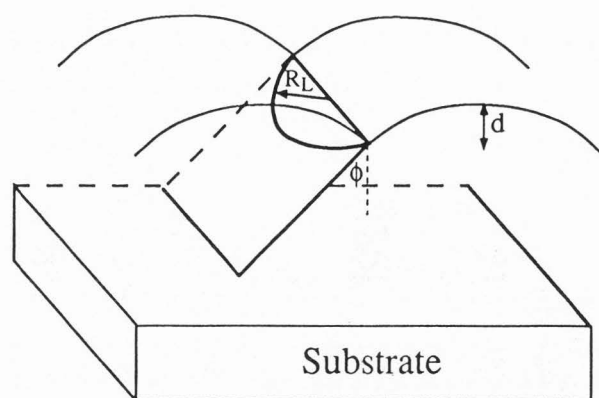


Figure 5. The geometry of dislocation half-loop emission at the tip of a surface cusp (see text).

the experimentally observed cusp depth of 7.5 nm. The Griffith criterion would, therefore, appear to describe the "unstable cusp geometry" at which the tip stress is beginning to accelerate rapidly. This is supported by recent theoretical studies (Chiu and Gao, 1993), which demonstrate that the stress fields of a slit crack and hypercycloid cusp are formally equivalent.

It is clear, however, that the large compressive stresses present at a cusp tip cannot directly lead to fracture. Rather, the likely mechanism of strain relief is the injection of misfit dislocations, which we consider further in the following section.

#### Nucleation of Misfit Dislocations

To model dislocation nucleation at a cusp tip, we have previously approximated the cusp stress field by the stress field of a crack (Jesson *et al.*, 1993a). In that analysis, only the dominant tensile component of the crack was considered. Here, we extend the analysis to include the other tensile and shear components and consider the nucleation of partial as well as complete dislocations. The geometry of half loop nucleation at a cusp tip is represented schematically in Figure 5. Following Jesson *et al.* (1993a), we write the total energy as a function of expanding loop radius  $R_L$  as,

$$U(R_L) = [R_L (b^2\mu/8) \{(2-\nu)/(1-\nu)\} \ln \{(\alpha R_L)/b\}] \\ - \{(R_L\mu b^2)/4\} \sin\beta + \{(\pi R_L^2)/2\} \delta \\ - C(R_L) \cos(\phi/2) \sin\phi \sin\beta. \quad (4)$$

The first term specifies the energy cost of a dislocation of core parameter  $\alpha$  and Burgers vector  $b$ . The second term describes the energy gained by the removal of a surface step,  $\beta$  being the angle between  $b$  and the dislocation line. The energy cost per unit area  $\delta$  of the

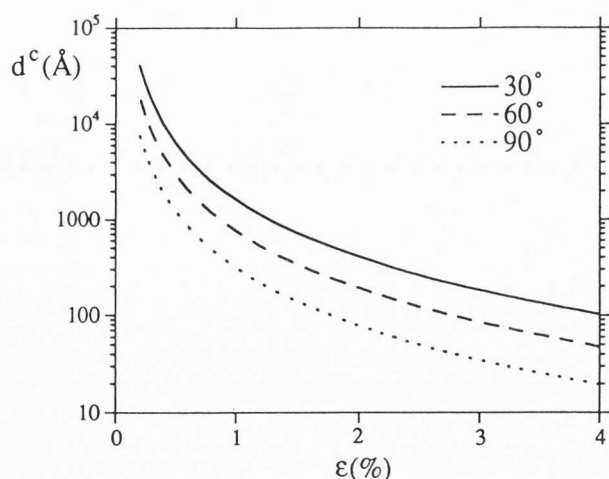


**Figure 6.** Critical cusp depth  $d^c$  required to nucleate  $30^\circ$ ,  $60^\circ$ , and  $90^\circ$  dislocations as a function of misfit  $\epsilon$  assuming an atomically sharp cusp. The curves are evaluated using eq. 6.

stacking fault associated with partial dislocations is included in the third term. The fourth term describes the elastic energy released by the loop, where the angle  $\phi$  is defined in Figure 5, and  $C(R_L)$  depends on the model used for the radial ( $R$ ) dependence of the stress field away from the tip. For the Westergaard sharp crack solution (Knott, 1973), we obtain

$$C(R_L) = 2.47 (d^{1/2}) R_L^{3/2} \mu \{(1+\nu)/(1-\nu)\} \epsilon b, \quad (5)$$

where  $\epsilon$  is the applied uniaxial strain and  $d$  is the crack depth (Fig. 5). From eq. 4, it is possible to determine the critical cusp depth  $d^c$  at which the activation barrier is equal to the available energy for nucleation [ $\sim 37$  kT (Kamat and Hirth, 1990)]. This leads to the simple condition for  $d^c$

$$\sqrt{d^c} \epsilon = A^\beta(T, \gamma), \quad (6)$$

where the constant  $A^\beta$  is dependent on the nature of the dislocation (i.e.,  $\beta = 30^\circ, 60^\circ$ , or  $90^\circ$ ), stacking fault energy, and temperature. For a given dislocation type,  $A^\beta(T, \gamma)$  can be estimated from a single energy calculation using eq. 4. The critical cusp geometry  $d^c$  is, therefore, simply related to misfit via eq. 6, and the results are summarized in Figure 6 using  $A^{30} = 0.402$ ,  $A^{60} = 0.276$ , and  $A^{90} = 0.177$ . The calculation pessimistically assumes a core parameter of 4 for all dislocation types.

An interesting feature of Figure 6 is that it is energetically more favorable to nucleate a complete  $60^\circ$  half loop from a cusp rather than a  $30^\circ$  partial. This is im-

portant because the glide plane geometry dictates that in compression, it is necessary to nucleate the  $30^\circ$  partial before the energetically favorable  $90^\circ$  partial. The nucleation of complete  $60^\circ$  dislocations is, therefore, favored in this case for atomically sharp cusps. It is interesting to compare half loop nucleation at cusps with half loop nucleation at flat surfaces, where it is only favorable to inject a complete  $60^\circ$  dislocation before a  $30^\circ$  partial if a step is removed. However, unlike the cusp, the energy barrier for the nucleation of a  $90^\circ$  partial is only lower than the  $60^\circ$  half loop barrier down to 1% misfit. At this point, the critical radius is very large, and the stacking fault energy correspondingly high. Note that in the case of a critical cusp geometry, the critical radius is always small, rendering the stacking fault energy less important.

The  $60^\circ$  curve in Figure 6 suggests that dislocation nucleation at the tip of an atomically sharp cusp is only likely for misfits somewhat larger than 1%. This is because the scale of morphological development associated with typical growth times is only of the order of a few hundred Angstroms at 1% misfit (Pidduck *et al.*, 1992).

The utilization of a sharp crack model for dislocation emission at a cusp tip can provide useful insight into the dislocation emission process. However, such a model is only valid if the critical radius  $R_c$  is significantly greater than the cusp radius of curvature  $\rho$  and appreciably less than the cusp depth  $d^c$ . Clearly, this is not true for very large misfits close to 4% involving small  $d$  and  $R_c$ . Furthermore, it is clear from our images that at 2% misfit the cusps are not atomically sharp so that the sharp crack solution is not strictly applicable. When the critical loop radius is of the order of the tip radius of curvature  $\rho$ , a more suitable model is the blunt crack approximation (Tetelman and McEvily, 1967) giving

$$C(R_L) = [2 \{(1+\nu)/(1-\nu)\} \epsilon \mu b d^{1/2}] \int_0^{R_L} [\{\rho + 4(R_L^2 - x^2)^{1/2}\}^{1/2} - \rho^{1/2}] dx. \quad (7)$$

The additional term

$$E(R_L) = -\pi R_L^2 \mu \{(1+\nu)/(1-\nu)\} \epsilon b \cos \lambda \cos \phi \quad (8)$$

associated with the mean elastic energy released by the loop must also be added to the right side of eq. 4 in the blunt crack model. Here,  $\lambda$  is the angle between  $\mathbf{b}$  and the direction in the interface perpendicular to the line of intersection of the slip plane and the interface. For a planar surface,  $\phi$  is the angle between the specimen surface and fault plane normal.

In Figure 7, we plot the total energy for nucleation of a  $60^\circ$  half loop in the blunt crack model as a function

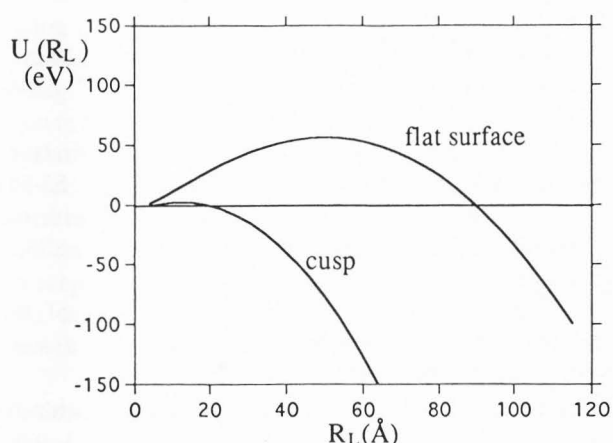


**Figure 7.** Plot of the total energy  $U(R_L)$  for  $60^\circ$  half loop nucleation as a function of expanding loop radius  $R_L$  on a blunt crack model. The top curve corresponds to nucleation at a flat surface and is associated with a large activation barrier. The lower curve involves nucleation at a cusp corresponding to our experimental geometry ( $\rho = 1.5$  nm,  $d = 7.5$  nm).

of expanding loop radius. For comparison, the top curve represents the familiar situation of nucleation at a flat surface where,

$$U(R_L) = [\mu b^2 R_L / 8] \{ (2-\nu)/(1-\nu) \} \ln \{ (\alpha R_L) / b \} - \pi R_L^2 \mu \{ (1+\nu)/(1-\nu) \} \epsilon b \cos \lambda \cos \phi. \quad (9)$$

As the loop expands,  $U(R_L)$  increases until a large activation barrier of 50 eV is encountered at a critical loop radius of 5 nm. Since the available thermal energy of 2 eV is considerably less than the energy barrier, it is effectively impossible to nucleate a  $60^\circ$  half-loop at a flat surface. However, if we consider a surface cusp of the geometry seen in our image, then the critical radius is reduced from 5 nm to 1.5 nm, of the same order as the cusp radius of curvature. Furthermore, the activation barrier is reduced to 2 eV, the available thermal energy, for  $\alpha = 3$  which is a very reasonable choice of core parameter in this system. Note that the blunt crack model conveys the important point that the critical cusp depths estimated from the sharp crack model in Figure 6 are likely to be significant overestimates. Although, the absolute stress concentration is naturally reduced at a blunt tip, the resolved shear stress field is significant over a larger region of the glide plane than in the case of a sharp crack. This can appreciably assist the nucleation process.

### Discussion

As noted earlier, the range of misfit over which

cusp nucleation is feasible can be estimated in the sharp crack approximation from the  $60^\circ$  curve in Figure 6. At low misfits, the maximum undulation amplitude is of the order of several tens of nanometers (Pidduck *et al.*, 1992). This limits the maximum stress concentration that can develop and suggests that cusp nucleation would be valid for misfits  $\geq 1.5\%$ . It is, however, conceivable that a blunt cusp tip might also be capable of operating as a dislocation nucleation source at even lower misfits. For example, it is apparent that undulations can occasionally reach depths of 65 nm at 0.76% misfit (Cullis *et al.*, 1994). Our calculations suggest that nucleation would require  $\rho = 8 \text{ \AA}$  ( $\alpha = 3$ ). Although such a tip geometry might eventually develop during growth, we would anticipate increasing competition from heterogeneous or other nucleation sources at lower misfits (see, for example, Perovic *et al.*, 1989, 1993).

The idea of dislocation nucleation at a cusp tip has important implications for the concept of critical thickness. In particular, it suggests a second kinetic critical thickness  $h_D$  associated with dislocation nucleation. This can be significantly greater than the equilibrium critical thickness  $h_c$  (Van der Merwe, 1963; Matthews, 1975) as sufficient time is required to generate a stress concentration capable of overcoming the large activation barriers associated with nucleation at a planar surface.

The nucleation of misfit dislocations at a cusp tip is clearly also connected with the question of ductile versus brittle behavior and the stability of cleavage cracks. It is interesting that the concept of crack blunting by dislocation emission, which is of relevance to crack stability, might also be relevant to the case of atomically sharp cusps if the emitted loop has a Burgers vector component normal to the plane containing the cusp line. This effect would tend to turn off the cusp source and would require further sharpening by stress enhanced surface diffusion before the emission of additional loops. Furthermore, several loops emitted on a given (111) plane will tend to produce a dislocation pileup at the substrate, creating a back stress at the cusp tip source. If the effective source stress is smaller than the threshold stress required to generate a single loop, then the source will shut down. It is conceivable that the cusp will then continue to develop (and possibly sharpen) during deposition, emitting further loops on different (111) planes. This role as a multiple source might explain why the cusp geometry appears to persist for 20 nm or so before rapidly flattening out as the mean strain in the film is eventually relieved.

### Conclusions

We have utilized Ge marker layer experiments combined with Z-contrast imaging to study the evolving sur-

face morphology of a  $\text{Si}_{0.5}\text{Ge}_{0.5}$  alloy. The transition between planar 2D growth and 3D growth is observed to occur at a kinetic critical thickness somewhat smaller than 25 nm. The slightly undulating surface is then observed to evolve into cusp-like surface instabilities as a result of stress-driven diffusion. These features become highly unstable at a critical geometry which appears to be intimately linked with the Griffith criterion for fracture. This then defines a second kinetic critical thickness  $h_D$ , which we believe is associated with dislocation nucleation at the cusp tip.

### Acknowledgments

We would like to thank S. L. Carney, T. C. Estes, and J. T. Luck for technical assistance. This research was sponsored by the Division of Materials Sciences, U.S. Department of Energy, under contract DE-AC05-84OR21400 with Martin Marietta Energy Systems, Inc.

### References

- Asaro RJ, Tiller WA (1972) Interface morphology development during stress corrosion cracking: Part I. Via surface diffusion. *Metall. Trans.* **3**, 1789–1796.
- Chason E, Tsao JY, Horn KM, Picraux ST, Atwater HA (1990) Surface roughening of Ge (001) during 200 eV Xe ion bombardment and Ge molecular beam epitaxy. *J. Vac. Sci. Technol. A* **8**, 2507–2511.
- Chiu C-H, Gao H (1993) Stress singularities along a cycloid rough surface. *Int. J. Solids Structures* **30**, 2983–3012.
- Chiu C-H, Gao H (1994) Numerical simulation of diffusion controlled surface evolution. *Mat. Res. Soc. Symp. Proc.* **317**, 369–374.
- Cullis AG, Robbins DJ, Barnett SJ, Pidduck AJ (1994) Growth ripples upon strained SiGe epitaxial layers on Si and misfit dislocation interactions. *J. Vac. Sci. Technol. A* **12**, 1924–1931.
- Gao H (1991) Stress concentrations at slightly undulating surfaces. *J. Mech. Phys. Solids* **39**, 443–458.
- Grinfeld MA (1986) Instability of the separation boundary between a non-hydrostatically stressed elastic body and a melt. *Sov. Phys. Dokl.* **31**, 831–834.
- Jesson DE, Pennycook SJ, Baribeau J-M, Houghton DC (1993a) Direct imaging of surface cusp evolution during strained layer epitaxy and implications for strain relaxation. *Phys. Rev. Lett.* **71**, 1744–1747.
- Jesson DE, Pennycook SJ, Baribeau J-M, Houghton DC (1993b) Evolving surface cusps during strained layer epitaxy. *Mat. Res. Soc. Symp. Proc.* **312**, 47–52.
- Jesson DE, Pennycook SJ, Baribeau J-M, Houghton DC (1994) Surface stress, morphological development, and dislocation nucleation during strained layer epitaxy. *Mat. Res. Soc. Symp. Proc.* **317**, 297–302.
- Kamat SV, Hirth JP (1990) Dislocation injection in strained multilayer structures. *J. Appl. Phys.* **67**, 6844–6850.
- Knott JF (1973) *Fundamentals of Fracture Mechanics*. John Wiley and Sons, New York. pp. 55–58.
- Matthews JW (1975) Defects associated with the accommodation of misfit between crystals. *J. Vac. Sci. Technol.* **12**, 126–133.
- Nozières P (1993) Amplitude expansion of the Grinfeld instability due to uniaxial stress at a solid surface. *J. de Physique* **3**, 681–686.
- Pennycook SJ, Jesson DE (1990) High-resolution incoherent imaging of crystals. *Phys. Rev. Lett.* **64**, 938–941.
- Pennycook SJ, Jesson DE (1991) High-resolution Z-contrast imaging of crystals. *Ultramicroscopy* **37**, 14–38.
- Perovic DD, Weatherly GC, Baribeau J-M, Houghton DC (1989) Heterogeneous nucleation sources in molecular beam-epitaxy grown  $\text{Ge}_x\text{Si}_{1-x}/\text{Si}$  strained layer superlattices. *Thin Solid Films* **183**, 141–156.
- Perovic DD, Houghton DC, Noël J-P, Rowell NL (1993) On the breakdown of layer-by-layer growth and the spontaneous nucleation of misfit dislocations in molecular-beam epitaxially grown GeSi/Si. *J. Vac. Sci. Technol. B* **11**, 889–891.
- Pidduck AJ, Robbins DJ, Cullis AG, Leong WY, Pitt AM (1992) Evolution of surface morphology and strain during SiGe epitaxy. *Thin Solid Films* **222**, 78–84.
- Spencer BJ, Meiron DI (1994) Nonlinear evolution of the stress-driven morphological instability in a two-dimensional semi-infinite solid. *Acta. Metall. Mater.* **42**, 3629–3641.
- Spencer BJ, Voorhees PW, Davies SH (1991) Morphological instability in epitaxially strained dislocation free solid films. *Phys. Rev. Lett.* **67**, 3696–3699.
- Spencer BJ, Voorhees PW, Davies SH (1993) Morphological instability in epitaxially strained dislocation free solid films: Linear stability theory. *J. Appl. Phys.* **73**, 4955–4970.
- Srolovitz DJ (1989) On the stability of surfaces of stressed solids. *Acta. Metall.* **37**, 621–625.
- Tetelman AS, McEvily AJ (1967) *Fracture of Structural Materials*. John Wiley and Sons, Inc., New York. p. 49.
- Van der Merwe JH (1963) Crystal interfaces. Part II. Finite overgrowths. *J. Appl. Phys.* **34**, 123–127.
- Yang WH, Srolovitz DJ (1993) Cracklike surface instabilities in stressed solids. *Phys. Rev. Lett.* **71**, 1593–1596.

### Discussion with Reviewers

**Reviewer I:** Have the authors considered that the obser-

vation of Figure 4 might be explained by invoking the Stranski-Krastanow growth mode; i.e., what they are seeing might be the coalescence of islands during growth?

**Authors:** Cusp formation is, of course, equivalent to the creation of intersection lines between islands. Such features form in Figure 4 within the context of far-from-equilibrium Stranski-Krastanow growth. The emphasis on cusps is particularly useful as it provides new insight into the nature and consequences of this important growth mode.

**Reviewer I:** The authors have used a value of 1.5 nm for the radius of curvature of the cusp in deriving the data presented in Figure 7. Where did this value come from? How are the results affected if larger (and perhaps more realistic) values are taken?

**Authors:** The value of the radius of curvature  $\rho$  measured from the micrograph is 3 nm. The accuracy of this measurement is limited by strain enhanced interdiffusion of the Ge marker layers, projection along a cusp line, and most importantly, the assumption that the marker layer corresponds to the spatial location where  $\rho$  is a minimum. All of these effects will tend to increase  $\rho$  so that the measured value can be regarded as an upper limit. As the tip stress varies only as  $\rho^{-1/2}$ , the results are not highly sensitive to the choice of  $\rho$ . We believe that a reduction of the measured value by a factor of two represents a conservative estimate.

**Reviewer I:** What is the thermodynamic driving force to form a sharp crack or cusp in a coherently strained layer which is under compression?

**Authors:** The thermodynamic driving force to form a cusp in a compressively strained layer relates to the energy gained by elastic deformation which, beyond a critical wavelength, exceeds the additional cost in surface energy.

**M. Grinfeld:** Is not the continuum approach too rough for attacking nano-scale problems?

**Authors:** Yes. We have recently found that surface steps and step interactions which are not explicitly included in the continuum theory can significantly change the conditions for instability. There would seem considerable scope, therefore, to refine the continuum theory in such a way as to relate more closely to the microscopic processes, which undoubtedly influence morphological instability.

**M. Grinfeld:** Could you suggest any precise definition of a kinetic critical thickness and the formula of it?

**Authors:** The kinetic critical thickness is the film thickness at which the perturbation grows more rapidly

than the rate at which the film thickens. Experimentally, this corresponds to the stage where the instability becomes apparent, and the measurement of this thickness will depend on both the resolution and nature of the experiment. A mathematical formula for the kinetic critical thickness, within the usual approximations of the continuum theory, has been given by Spencer *et al.* (1994) as

$$\sigma(\bar{h}) > \{V/\bar{h}(t)\}$$

where  $\bar{h}$  is the mean film thickness,  $V$  is the growth velocity of the planar film and  $\sigma(\bar{h})$  is the static film perturbation growth rate.